Caroline Van der Heyden[1,2]
Bart Vanthillo[1]
Jan G. Pieters[1]
Peter Demeyer[2]
Eveline I. P. Volcke[1]

[1]Department of Biosystems Engineering, Ghent University, Ghent, Belgium.

[2]Unit Technology and Food, Institute for Agricultural and Fisheries Research, Merelbeke, Belgium.

Mechanistic Modeling of Pollutant Removal, Temperature, and Evaporation in Chemical Air Scrubbers

Chemical air scrubbers reduce the concentration of water-soluble components such as ammonia from the outgoing ventilation air through absorption in water, followed by chemical conversions and removal of the end products. A mechanistic model for a countercurrent air scrubber was set up. Mass balances for ammonia, hydrogen sulfide, nitrous oxide, and methane were implemented, as well as the water mass balance and heat balances. The model was validated against experimental data from a conventional fattening pig housing facility. The effect of influent characteristics, design parameters, and control handles on the removal efficiency, the temperature profile, and the water evaporation rate were investigated through simulation. The model was able to describe the behavior of a countercurrent chemical air scrubber.

Keywords: Air scrubber, Heat transfer, Mass transfer, Process design, Process modeling

Received: November 3, 2015; *revised:* January 19, 2016; *accepted:* May 10, 2016

DOI: 10.1002/ceat.201500664

Supporting Information available online

1 Introduction

Chemical air scrubbers are widely applied for air pollution control. They are used to efficiently remove pollutants from the gas stream through absorption, typically in water, followed by chemical conversions and removal of the end products. The working principle of this type of air scrubbers has already been extensively discussed in the literature by other authors [1–3]. Applications comprise exhaust streams containing SO_2 and NO from combustion plants [4, 5], chlorine gas streams [6], or streams from agricultural applications containing mainly ammonia [7–10]. Optimal reactive absorption can be achieved by correct process design, which is mainly dependent on proper packing selection and thorough understanding of the process behavior. For the latter purpose, the application of reliable and adequate process models is widespread [11]. Useful models can be found in the literature for many chemical air scrubber applications, such as the desulfurization process [12–14], the absorption of odorous compounds [15, 16], and the absorption of ammonia in water using different scrubbing systems [17–22]. However, none of these models consider the pollutant removal efficiency simultaneously with temperature and water evaporation, which is essential to assess the interaction between the scrubber performance, the temperature dynamics, and the water consumption.

The objective of this work was to set up a mechanistic model capable of predicting the pollutant removal efficiency, air temperature, and relative humidity distribution over the packed bed. The mass transfer of chemical species was taken into account, as well as heat transfer considering both sensible and latent heat exchange. Additionally, various correlations to calculate the mass transfer coefficient, which is the most important parameter in absorption models, were investigated in more detail.

The model was validated using the experimental data of a chemical countercurrent air scrubber installed at a conventional fattening pig housing facility, for ammonia removal, air temperature, and relative humidity distribution. A case study was defined, considering a chemical air scrubber at a conventional fattening pig housing facility with 1000 animal places. In the first place, typically prevailing parameters and variables of the case study were used to simulate the (steady-state) reference case. Subsequently, the effects of the typical variations in ventilation rate, incoming pollutant concentrations (loads), air temperature, and relative humidity on the removal efficiency, the temperature profile over the packing, and the evaporation rate were studied. The effects of important design parameters of air scrubbers such as the packing characteristics and the packing dimensions, as well as of important operational variables in air scrubbers, such as the pH of the washing water and the liquid flow rate, were assessed as well.

2 Model Description

2.1 Model Setup

The mechanistic model (Fig. 1) was developed for a countercurrent chemical air scrubber and was implemented in Matlab-Simulink®. The packing material was represented by a

Correspondence: Caroline Van der Heyden (Caroline.VanderHeyden@UGent.be), Department of Biosystems Engineering, Ghent University, Coupure links 653, 9000 Gent, Belgium.

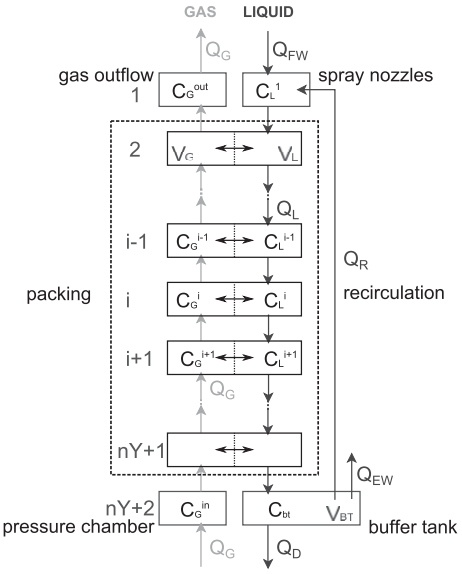

Figure 1. Schematic overview of the mechanistic model for a countercurrent chemical air scrubber.

sufficiently high number of horizontal cells consisting of an air phase and a liquid phase, separated by a stagnant boundary layer at the interface (two-film theory) and both of which were represented by ideally mixed continuous stirred-tank reactors (CSTR) placed in series. In each horizontal layer, a homogeneous distribution of the incoming ventilation air and spraying water is assumed, meaning that neither concentration nor temperature gradients were considered along the horizontal axis. This results in a one-dimensional model, reducing complexity and calculation time. The liquid buffer tank was modeled as a separate ideally mixed reactor cell. The liquid phase of the top cell is fed by the incoming washing liquid from the buffer tank, distributed in practice by the spray nozzles. The gas phase of the top cell contains the outgoing clean air, flowing out from the air scrubber. It was assumed that no mass transfer between the gas and liquid phases took place in this cell. The bottom cell contains the incoming exhaust air and the washing liquid in the buffer tank, which is the only CSTR that has a larger liquid volume than the other cells. Also for this cell, it was assumed that there was no mass transfer between the gas and liquid phases, because the prevailing specific exchange surface area is much smaller than in the packing material itself.

2.2 Mass Transfer

Mass transport was modeled by advection (plug flow) in the gas and liquid bulk phases. The resistance to transfer of the pollutants between the bulk gas and the bulk liquid was considered to be entirely located in the boundary layer; beyond the boundary layer, the turbulence is sufficient to eliminate concentration gradients [23]. Despite the simplification [24], plug flow was assumed for both concentrations and temperature, which could be justified in air scrubbers due to the high Peclet numbers ($Pe = h_p u \rho c_p/\lambda > 10$)[1)] and the high air velocities typically prevailing in these systems [25]. Dispersion or channeling phenomena were not considered in the model [26].

Equilibrium between the gas and the liquid phase was assumed at the interface, making Henry's law applicable. It was assumed that no reactions took place in the gas phase. Adsorption of pollutants to the inert packing material was neglected. Ionic strength could have an effect on the ammonia removal as the acidity constant and the Henry coefficient depend on this parameter [27]. However, it was not implemented in the model in order to reduce complexity [28]. Liu et al. [29] investigated the influence of ionic strength on the removal of odorous components and found that it was negligible.

The individual gas and liquid phase mass balances for a pollutant (index is omitted for simplicity) in cell i were implemented as

$$\frac{dC_G^i}{dt} = \frac{Q_G}{V_{G,cell}}\left(C_G^{i+1} - C_G^i\right) - K_L^i\left[T_G^i, T_L^i\right] a\left(\frac{C_G^i}{H^i\left[T_G^i, T_L^i\right]} - C_L^i\right) \quad (1)$$

$$\frac{dC_L^i}{dt} = \frac{Q_L}{V_{L,cell}}\left(C_L^{i-1} - C_L^i\right) + K_L^i\left[T_G^i, T_L^i\right] a\left(\frac{C_G^i}{H^i\left[T_G^i, T_L^i\right]} - C_L^i\right) \quad (2)$$

respectively, expressing that the accumulation or depletion of a pollutant in the gas phase in cell i is due to the influx from the underlying cell with concentration C_G^{i+1} and the outflow to the overlying cell with concentration C_G^i, as well as transfer of this pollutant from the gas phase to the liquid phase or vice versa. K_L is the total mass transfer coefficient, considering the resistances at the liquid and gas interface. The larger K_L and the specific surface area a, the more pollutant is removed from the gas phase. The Henry coefficient H, valid for dilute systems, expresses the ratio of the gas concentration to the liquid concentration at the interphase surface area, considered to be at equilibrium. In the liquid phase, the total lumped concentration of a pollutant was divided into both considered species, e.g., ammonia and ammonium, based on the acidity constant K_a and the pH of the washing water. A constant pH was assumed throughout the reactor. The temperature dependencies of the Henry coefficient and the acidity constant are expressed in Tab. S1 in the Supporting Information.

2.3 Heat Transfer

The temperature distribution in the air scrubber was determined by the heat exchange in each cell due to the sensible heat exchange and the latent heat exchange due to water evaporation, assuming a perfectly adiabatic reactor. It was assumed that the heat for evaporation was in the first place provided by the

1) List of symbols at the end of the paper.

liquid phase while the energy to heat up the newly formed water vapor was considered to be withdrawn from the gas phase. The heat of solution of the different pollutants was neglected as their transferred amount is relatively low. The individual gas and liquid phase energy balances in cell i thus read as

$$\frac{dT_G^i}{dt} = \frac{Q_G}{V_{G,cell}}\left(T_G^{i+1} - T_G^i\right) - h^i\left[T_G^i, T_L^i\right]a\left(T_G^i - T_L^i\right) - \frac{k_{G,H_2O}^i\left[T_G^i\right]a\left(\rho_{int}^i\left[T_G^i, T_L^i\right] - \rho_v^i\left[T_G^i\right]\right)c_{p,st}\left(T_G^i - T_L^i\right)}{\rho_G^i\left[T_G^i\right]c_{p,G}} \quad (3)$$

$$\frac{dT_L^i}{dt} = \frac{Q_L}{V_{L,cell}}\left(T_L^{i-1} - T_L^i\right) + h^i\left[T_G^i, T_L^i\right]a\left(T_G^i - T_L^i\right) - \frac{k_{G,H_2O}^i\left[T_G^i\right]a\left(\rho_{int}^i\left[T_G^i, T_L^i\right] - \rho_v^i\left[T_G^i\right]\right)\Delta H_V^i}{\rho_L c_{p,L}} \quad (4)$$

respectively. The first term in both equations denotes the advective transport of heat between the cells, the second term the sensible heat exchange, and the third term the latent heat exchange in the cell. h is the total heat transfer coefficient ($W\,m^{-2}K^{-1}$), considering the resistances at the liquid and gas interface.

2.4 Water Balance and Evaporation Rate

The evaporation of water in a nonsaturated environment involves the coupling of mass and heat transfer. The water balance was expressed in terms of the water vapor density ρ_v ($kg\,m^{-3}$), of which the accumulation in the gas phase reads as:

$$V_{G,cell}\frac{d\rho_v^i}{dt} = Q_G\left(\rho_v^{i+1} - \rho_v^i\right) - k_{G,H_2O}^i\left[T_G^i\right]a\left(\rho_{v,int}^i\left[T_G^i, T_L^i\right] - \rho_v^i\left[T_G^i\right]\right) \quad (5)$$

with k_{G,H_2O} being the mass transfer coefficient at the gas side ($m\,s^{-1}$) and ρ_{int} the water vapor density at the interphase ($kg\,m^{-3}$). The first term represents the advective transport of water vapor between the cells, the second one the transfer of water vapor between the gas and the liquid phase in the cell. The amount of water evaporated in each cell per time instant was negligible, allowing the assumption that the volume of the liquid phase was the same for all cells along the packing material (see the Supporting Information).

The water vapor density of the incoming air (ρ_v^{in}) was calculated from the ideal gas law (Eq. (6)). Its vapor pressure (p_v^{in}, Eq. (7)) was calculated based on the incoming relative humidity (RH) and the saturated vapor pressure (p_{sv}^{in}), which is dependent on the incoming air temperature (see the Supporting Information).

$$\rho_v^{in} = \frac{p_v^{in}M_{H_2O}}{R\left(T_G^{in} + 273.15\right) \times 1000\ g\,kg^{-1}} \quad (6)$$

$$p_v^{in} = \frac{RH^{in}}{100}p_{sv}^{in}\left[T_G^i\right] \quad (7)$$

The flow rate of water evaporating was calculated based on the difference in water vapor density between the cell containing the outgoing air and the cell containing the ingoing air.

$$Q_{EW} = Q_G\frac{1}{\rho_L^1}\left(\rho_v^1 - \rho_v^{in}\right) \quad (8)$$

The total water consumption was not only dependent on the evaporation rate but also on the amount of discharged water (Q_D). Both need to be replaced to maintain a constant water volume in the buffer tank.

2.5 Mass and Heat Transfer Coefficient Calculation

The total mass transfer coefficient K_L in Eqs. (1) and (2) is determined including both diffusion and convection, taking into account the resistance to mass transfer at the gas and the liquid boundary layers. This total mass transfer resistance is characterized by the mass transfer coefficients in the gas and liquid phases (k_G and k_L, respectively) and the Henry coefficient (H) according to the generally applied two-film theory [30]:

$$\frac{1}{K_L^i} = \frac{1}{H^i k_G^i} + \frac{1}{k_L^i} \quad (9)$$

Both the gas and liquid phases can constitute significant mass transfer resistances [30–32]. The Henry coefficient has a large impact on whether the mass transfer for a given contaminant is limited by the gas side resistance, the liquid side resistance, or both [33]. The transfer of highly soluble compounds (low H) is generally limited by the gas side resistance, while highly volatile compounds (high H) are mostly limited by the liquid side resistance [34]. Typical values for a countercurrent packed scrubber with a specific surface area between 10 and $350\,m^2m^{-3}$ lie between 7.5×10^{-4} and $5.0\times10^{-2}\,m\,s^{-1}$ for k_G and between 4×10^{-5} and $2\times10^{-4}\,m\,s^{-1}$ for k_L [16]. To adequately describe both highly soluble compounds and highly volatile compounds in this model, both gas and liquid mass transfer were taken into account. Besides pollutants, the transfer of water between the gas and liquid phase was considered as well. The total convective mass transfer coefficient for water is completely determined by the mass transfer coefficient for the gas phase, as the one for the liquid phase is infinitely large ($k_{L,H_2O} \approx \infty$).

The mass transfer coefficients for the gas and liquid phases (F is L or G) are defined as the ratio between the diffusion coefficient (D) and the thickness of the film (y) (Eq. (10)).

$$k_F^i = \frac{D_F^i}{y_F} \quad (10)$$

As the thickness of the film is not known, empirical correlations are typically used to determine the mass transfer coefficient [32]. The accuracy of these correlations usually lies around 30 %, but larger errors are not uncommon [35]. The correlations are useful for the preliminary design of small pilot plants, but should always be checked experimentally before the actual construction of a full-scale plant. To understand the behavior of air scrubbers, the use of these correlations in the

model is very convenient and can be accepted. Various correlations to calculate the gas and liquid mass transfer coefficient are available in the literature. The dimensionless form of the correlations for the mass transfer coefficient may disguise the very real qualitative similarities between them. They are typically dependent on the Reynolds number (*Re*) and the Schmidt number (*Sc*) [32]. Additionally, they are dependent on the shape and structure of the considered random or structured packing materials. The packing was further assumed to be completely wetted (no dry spots), for reasons of simplicity and generality of the model. In practice, the wetted specific surface area may be somewhat lower and can be calculated from correlations that highly depend on the specific packing characteristics [32].

Fig. 2 compares the values of mass and heat transfer coefficients obtained with three frequently used correlations for randomly or structured packed countercurrent columns (see Sect. S2), namely those of Onda et al. [36], Shulman et al. [37], and Billet and Schultes [38] for three different types of packing material. The heat transfer coefficient was calculated from the mass transfer coefficient, using the heat and mass transfer analogy of Chilton and Colburn [39]:

$$\frac{Sh}{Nu} = \left(\frac{Sc}{\mathrm{Pr}}\right)^{m} \tag{11}$$

with *Sh* being the Sherwood number, *Nu* the Nusselt number, *Sc* the Schmidt number, and *Pr* the Prandtl number. The power coefficient *m* is set at 1/3 for most configurations.

For all shown correlations, except for the one of Onda et al. [36], the mass and heat transfer coefficients increase with increasing specific surface area. The heat transfer coefficient calculated with the correlation of Onda et al. [36] lies around 4000 $\mathrm{W\,m^{-2}K^{-1}}$, which is one order of magnitude higher than with the other correlations. Since the correlation of Billet and Schultes [38] was found to be the most flexible correlation and valid for different packing materials, this one was incorporated in the model:

$$k_{\mathrm{G}}^{i} = cp_{\mathrm{G}} \frac{a^{0.5} D_{\mathrm{G}}^{i}\left[T_{\mathrm{G}}^{i}\right]}{\sqrt{d_{\mathrm{h}}(\varepsilon - h_{\mathrm{L}})}} \left(\frac{\rho_{\mathrm{G}}^{i}\left[T_{\mathrm{G}}^{i}\right] u_{\mathrm{G}}}{a\mu_{\mathrm{G}}^{i}\left[T_{\mathrm{G}}^{i}\right]}\right)^{3/4} Sc\left[T_{\mathrm{G}}^{i}\right]^{1/3} \tag{12}$$

$$k_{\mathrm{L}} = cp_{\mathrm{L}} \left(\frac{\mu_{\mathrm{L}}\left[T_{\mathrm{L}}^{i}\right] g}{\rho_{\mathrm{L}}}\right)^{1/6} \left(\frac{D_{\mathrm{L}}\left[T_{\mathrm{L}}^{i}\right]}{d_{\mathrm{h}}}\right)^{0.5} \left(\frac{u_{\mathrm{L}}}{a}\right)^{1/3} \tag{13}$$

where d_{h} is the hydraulic diameter of the packing material and h_{L} is the liquid holdup of the packing, calculated according to [38]:

$$d_{\mathrm{h}} = 4\frac{\varepsilon}{a} \tag{14}$$

$$h_{\mathrm{L}} = \left(12 \frac{1}{g} \frac{\mu_{\mathrm{L}}}{\rho_{\mathrm{L}}} u_{\mathrm{L}} a^{2}\right)^{1/6} \tag{15}$$

3 Case Study

A chemical air scrubber was considered to treat the exhaust air from a conventional fattening pig housing facility with 1000 animal places (Tab. 1). The components considered in the gas phase were ammonia as the most important component in the exhaust air from piggery houses [40], hydrogen sulfide as a model component that can be linked with odor removal [41], nitrous oxide and methane for their greenhouse potential, and water for the evaporation rate and temperature predictions. The considered incoming concentrations are based on typical

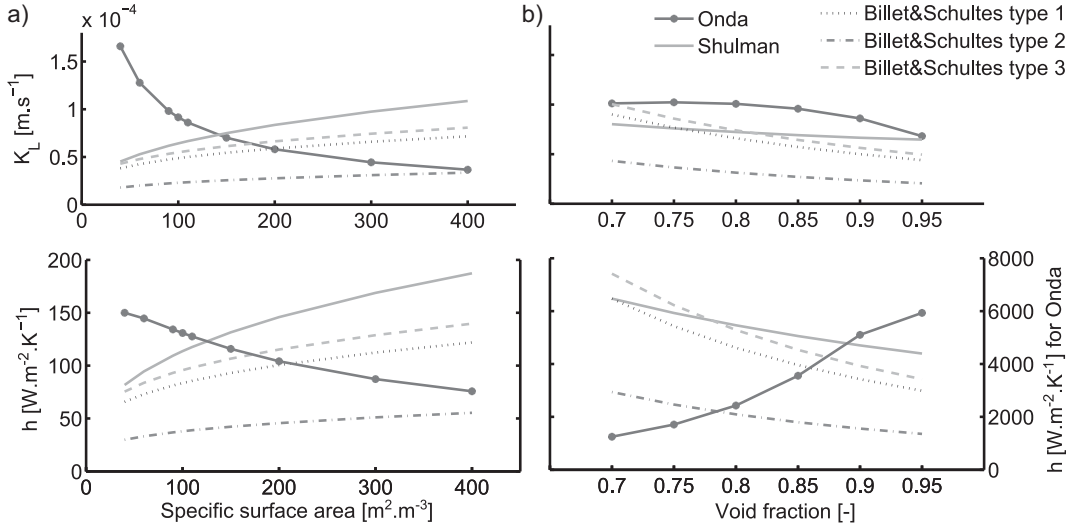

Figure 2. Comparison of K_{L} for ammonia and *h* values for the correlations of Onda et al. [36], Shulman et al. [37], and Billet and Schultes [38] for three different types of packing materials in terms of (a) specific surface area *a* ($\mathrm{m^2m^{-3}}$) with a void fraction of 0.90 and (b) void fraction of the packing material with a specific surface area of 110 $\mathrm{m^2m^{-3}}$. The values for cp_{G} and cp_{L} for type 1 (plastic dumped Pall rings of 50 mm) are 0.368 and 1.239, for type 2 (plastic Euroform) 0.167 and 0.973, and for type 3 (metal Montz packing B2-300) 0.422 and 1.165, respectively.

Table 1. Air scrubber design specifications and operational parameters.[a)]

Parameter	Symbol	Unit	Reference case		Scenario analysis			
					Min		Max	
Influent characteristics								
Number of pigs	n_{pigs}	[animal]	1000					
Ammonia load	EF_{NH3}	[kg_{NH3} $animal^{-1}a^{-1}$]	3	[38]	0.5	[38]	6.8	[38]
Incoming H_2S concentration	$C^{in}_{H_2S}$	[ppm]	1	[39]				
Incoming N_2O concentration	$C^{in}_{N_2O}$	[ppm]	1	[40]				
Incoming CH_4 concentration	$C^{in}_{CH_4}$	[ppm]	100	[40]				
Ventilation rate	Q_{vent}	[$m^3animal^{-1}h^{-1}$]	35		6	[41]	80	[41]
Gas exhaust temperature	T^{in}_G	[°C]	22.4	[42]	15		35	
Relative humidity	RH^{in}	[%]	65	[43]	45		99	
Design aspects								
Packing height	h_P	[m]	0.90		0.3		2.5	
Packing length	l_P	[m]	3				>	
Packing width	w_P	[m]	2					
Cross-sectional area	$A_{LW} = l_p w_P$	[m^2]	6		1		16.5	
Buffer tank height	h_{BT}	[m]	0.30					
Specific surface area	a	[m^2m^{-3}]	110	[33]	40		300	
Void fraction	ε	[–]	0.936	[33]	75		99	
Packing specific gas coefficient	cp_G	[–]	0.167	[33]				
Packing specific liquid coefficient	cp_L	[–]	0.973	[33]				
Operational aspects								
pH washing water	pH	[–]	4	[3]	2		14	
Water flow rate	Q_L	[$m^3h^{-1}m^{-2}$]	10	[3]	0.5		30	
Recirculation fraction	f_R	[%]	100	[3]	60		100	

[a)] All values without a reference are based on practical experience. The given minimum and maximum values indicate the range wherein the effects of the parameters on the removal efficiency and evaporation rate were tested (scenario analysis).

values found in the exhaust air of fattening pig housing facilities. The components considered in the liquid phase were ammonia (NH_3) and ammonium (NH_4^+), lumped into total ammonia nitrogen (TAN), and taking into account the chemical equilibrium between both species, hydrogen sulfide (H_2S) and the hydrosulfide ion (HS^-), lumped into total sulfide (TS), nitrous oxide (N_2O), and methane (CH_4).

The dimensions of the considered air scrubber were based on typical minimal empty bed residence times (EBRT) for ammonia removal in chemical air scrubbers, with an average value of 0.4 s [10, 42], corresponding to a minimum packing volume of 6.7 m^3 for the given number of pigs and the typically applied maximum ventilation rate for design purposes of 60 $m^3animal^{-1}h^{-1}$.

An acid was added to the washing water to decrease the pH, which results in an increase in the driving force for ammonia absorption. The pH value of the washing water was assumed to be constant, at a value of 4 for the reference case. The liquid flow rate Q_L was set to 10 $m^3h^{-1}m^{-2}$ cross-sectional area [3]. The recirculation rate was set to 100 % to reduce the water consumption. The washing water is recirculated until its ammonium concentration becomes too concentrated, which is in practice typically controlled on a time basis or through monitoring the electrical conductivity (EC) [3]. A maximum ammonium concentration of 30 $g_N L^{-1}$ is mostly reached in the washing water [3] and in the reference case it is assumed as set point. At discharge, one-third of the buffer tank was discharged and replaced with fresh water. Initially, the liquid phase contained no pollutants.

The typically prevailing parameters and variables of the case study were used to first simulate the (steady-state) reference case. Subsequently, a scenario analysis was performed, assessing the effect of the influent characteristics, important design aspects, and important operational aspects in air scrubbers.

4 Model Validation Based on Experimental Data

Experimental data were obtained during 35 h in June 2014 from a chemical air scrubber installed on a fattening pig housing facility for 1250 animals. NH_3 concentrations were measured using an Innova photoacoustic gas monitor 1314 connected to a CBISS multipoint sampler (LumaSense Technologies, Denmark). Samples were taken on average every 20 min sequentially at five sampling points: one point to measure the ingoing air and four points to measure the outgoing air of the scrubber to take into account a possible heterogeneous distribution of the removal over the packing. Each sampling consisted of at least six consecutive measurements with a 3-min time interval. Only the last stable measurement was taken into account to overcome a possible measuring delay of the gas monitor. A measurement was considered stable when the last two consecutively measured concentrations showed at most 5 % difference. The removal efficiency was calculated based on the average of the four outgoing sampling points and the subsequently measured incoming concentration. It should be noted that this implies a time difference between the measured incoming and outgoing concentrations of maximally 1 h and 24 min.

The ventilation rate was monitored through pressure difference measurements over the ventilation fans using a P26 differential pressure transducer (Halstrup-Walcher, Germany). The correlation between the pressure drop and the ventilation rate data was estimated using the ventilation computer readings. The pH and *EC* of the washing water were determined by chemical analysis at the beginning of the measuring campaign (Tab. 2). Dimensions and operating parameters of the chemical air scrubber were received from the air scrubber supplier.

The model was first validated for ammonia removal, air temperature, and relative humidity distribution using the experimental data of a chemical countercurrent air scrubber. The measurements for the ingoing ammonia concentration, air temperature, relative humidity, and ventilation rate were used as input for the simulation. The initial conditions for the simulation were set to the steady-state conditions corresponding with the influent conditions at that time instant.

Table 2. Characteristics of the chemical air scrubber in the measuring campaign.

Parameter	Symbol	Unit	Value
Packing height	h_p	[m]	0.38
Packing length	l_p	[m]	2.25
Packing width	w_p	[m]	5.46
pH washing water	pH	[–]	3.19[a)]
EC washing water	EC	[mS cm^{-1}]	100.9[a)]
Water flow rate	Q_L	[m^{3}h^{-1}m^{-2}]	10
Recirculation fraction	f_R	[%]	100

[a)] Sample taken on June 16, 2014, 2.15 pm.

5 Results and Discussion

5.1 Model Validation

The measured ingoing ammonia concentration varied between 18.1 and 23.6 ppm, depending on the ventilation rate (Fig. 3). For instance, at noon, when the animal activity is the highest and the indoor temperature increases, a higher ventilation rate is applied, resulting in a lower ammonia concentration entering the air scrubber. The ammonia concentration in the air scrubber decreased to an average outgoing ammonia concentration of 8.2 ± 1.2 ppm. The simulated outgoing ammonia concentration amounted to 7.4 ± 0.6 ppm and followed the experimental effluent ammonia concentration with, on average, 14 % difference, within one standard deviation of the measurements.

The temperature of the incoming exhaust gas remained almost constant at 24.8 ± 0.4 °C and decreased by approximately 5 °C throughout the scrubber to an exhaust temperature of 20.1 ± 2.5 °C. Such a temperature drop is typical of this type of systems [43, 44]. The simulated outgoing temperature was also 5 °C lower than the influent temperature and followed the measured outgoing air temperature profile well. The outgoing temperature is higher at a higher ventilation rate because more thermal mass enters the air scrubber. The maximum under- and overestimation were 9.2 and 16.7 %, respectively, with an average difference of only 2.0 %.

The measured relative humidity changed from an incoming value of 54.2 ± 3.4 % to an outgoing value of 87.1 ± 9.0 %. This latter value shows a large variation between 64.1 and 95.5 %. The simulation results of the relative humidity showed a rather constant value of 87.1 ± 1.2 %. In comparison, the simulated and modeled outgoing relative humidity had a 5 % average difference. The larger variation in the relative humidity measurements than in the simulated results can be attributed to the weather conditions, influencing the sensor that was placed outside the air scrubber. Overall, the model was well able to predict the outgoing ammonia concentration, temperature, and relative humidity.

5.2 Reference Case

The steady-state profiles over the air scrubber for the reference case are displayed in Fig. 4. The gas phase ammonia concentration decreased from 0.008 g_N m^{-3} (14 ppm) at the scrubber inlet to 0.0013 g_N m^{-3} (2.1 ppm) at the scrubber outlet, corresponding to a removal efficiency of 84 %. The odorous component H_2S and the greenhouse gases N_2O and CH_4 were hardly removed in the air scrubber (results not shown). This holds true for all components with a low solubility in water (high Henry coefficient). The relative humidity of the exhaust air gradually

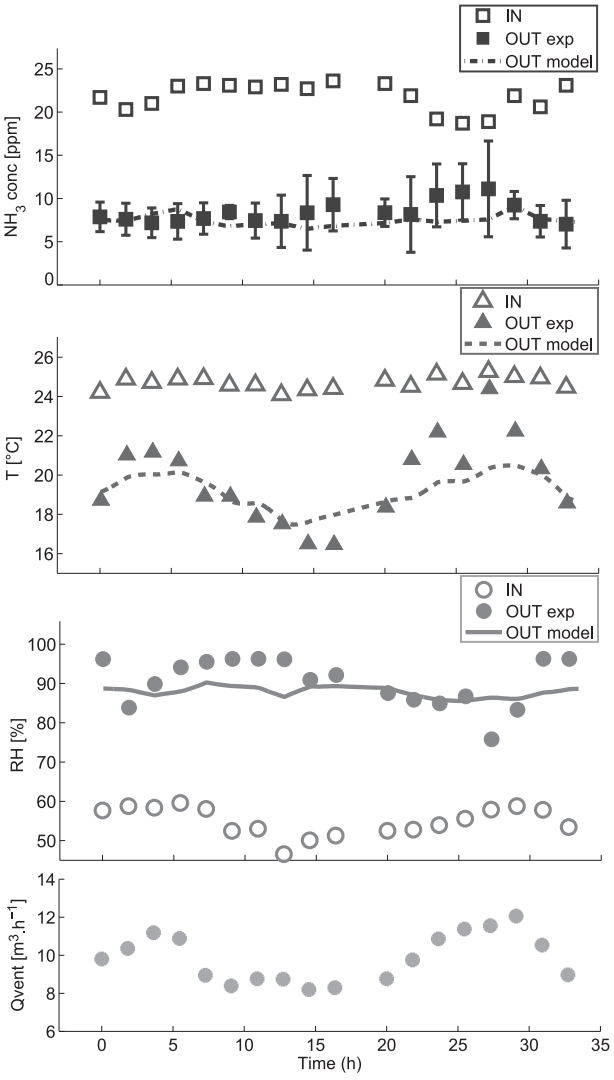

Figure 3. Comparison between experimental data and model simulation results for (a) the ammonia concentration, (b) the air temperature, and (c) the relative humidity, applying (d) the incoming ventilation rate as a simulation input.

increased while flowing through the air scrubber from 65 to 90 %, due to evaporation of the washing water. The assumption of a constant liquid cell volume in the packing regardless of the evaporation of water was justified as the calculated maximum evaporation under extreme conditions (35 °C and a relative humidity of 45 %) only led to a decrease of the water volume in the packing of 0.26 % (see Sect. S3). Through contact with the colder washing water, the gas temperature decreased from 22.4 to 18.0 °C, close to the wet bulb temperature of 17.9 °C. The liquid temperature slightly increased with the liquid flowing down through the air scrubber (Fig. 4 c). This small increase was cancelled due to evaporation in the lower part of the scrubber, and the liquid equilibrium temperature of 17.1 °C was reached again.

Despite an increasing ammonia concentration in the buffer tank (by 760 $g_N\,m^{-3}d^{-1}$, results not shown), the gaseous ammonia profile inside the air scrubber and thus the removal efficiency remained constant as the driving force was still high enough. To keep the ammonia concentration in the washing water below 30 $g_N\,L^{-1}$, the first discharge will take place after 40 d. If one-third of the water is discharged and replaced by fresh water, this means that every 13 d the threshold will be reached again. Under the constant conditions assumed in this case study, the yearly water loss due to evaporation amounted to 628 m^3, which is comparable to values found in full-scale countercurrent chemical air scrubbers [45, 46].

5.3 Influence of Influent Characteristics

5.3.1 Ventilation Rate, Pollutant Concentration, and Pollutant Load

The ventilation rate shows diurnal as well as seasonal variations at animal housing facilities. Typically, high concentrations will occur during winter and at night when the ventilation rate is low, and low concentrations will prevail in summer and during noon when the ventilation rate is at its maximum to remove excess heat [7, 47]. Figs. 5 a and d show the simulation result of a varying ventilation rate on the ammonia concentration in the air scrubber and on the ammonia removal efficiency, respectively. Assuming a constant emission factor, i.e., a constant incoming ammonia load, an increased ventilation rate implies a decreasing incoming ammonia concentration (Fig. 5 a). Nevertheless, the outgoing ammonia concentration increased for higher ventilation rates (Fig. 5 a), resulting in a decreasing removal efficiency (Fig. 5 d). Decreasing the incoming ammonia concentration while maintaining a constant ventilation rate did not affect the removal efficiency (Fig. 5 e) since the effluent ammonia concentration decreased according to the lower incoming load (Fig. 5 b). Increasing the ventilation rate while keeping the incoming ammonia concentration constant (Fig. 5 c) led to the same decrease in removal efficiency as observed for a constant ammonia load, indicating that the decrease of the ammonia removal efficiency at higher ventilation rates was only caused by the decrease in contact time rather than by a decreasing incoming ammonia concentration (Fig. 5 f).

A higher ventilation rate also implied that more water evaporated (results not shown), because of the increased incoming thermal mass and the higher velocity resulting in a higher mass transfer coefficient. Additionally, the simulated gas temperature decreased less with higher flow rates because of shorter contact times and the larger air mass coming into the scrubber. Through this increase in incoming thermal mass, higher liquid temperatures were modeled in the lower part of the scrubber, resulting in an increase of the temperature in the buffer tank.

5.3.2 Air Temperature

The simulated influence of the air temperature on the pollutant removal efficiency was found negligible in this case (only 0.1 % for a 20 °C change in air temperature, results not shown). With increasing air temperature, the gas pollutants will be less solu-

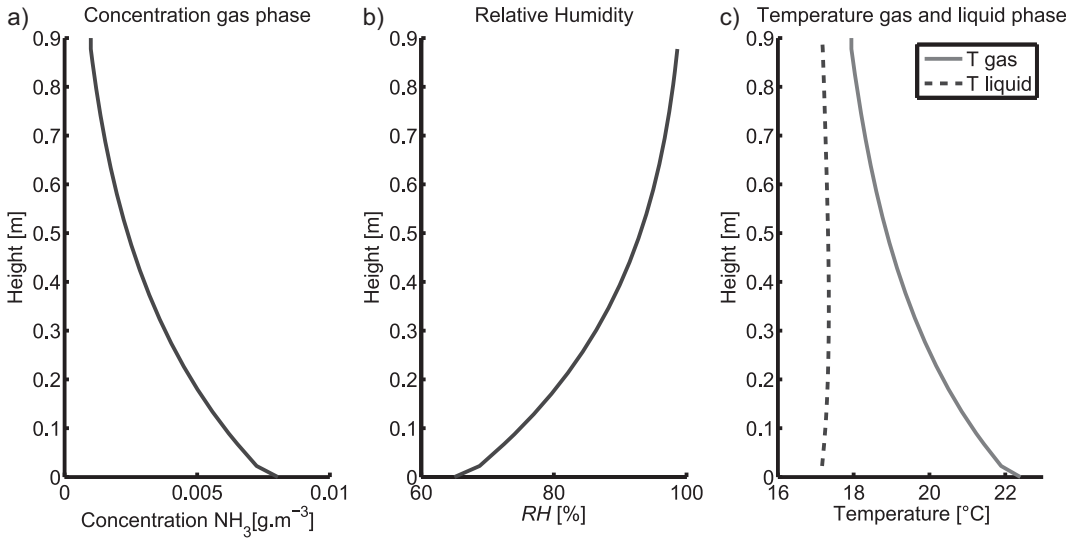

Figure 4. Simulated steady-state profiles in the air scrubber for (a) ammonia in the gas phase, (b) the relative humidity, and (c) the temperatures of the gas and liquid phases. The scrubber inlet and outlet correspond to position 0 and 0.9 m, respectively.

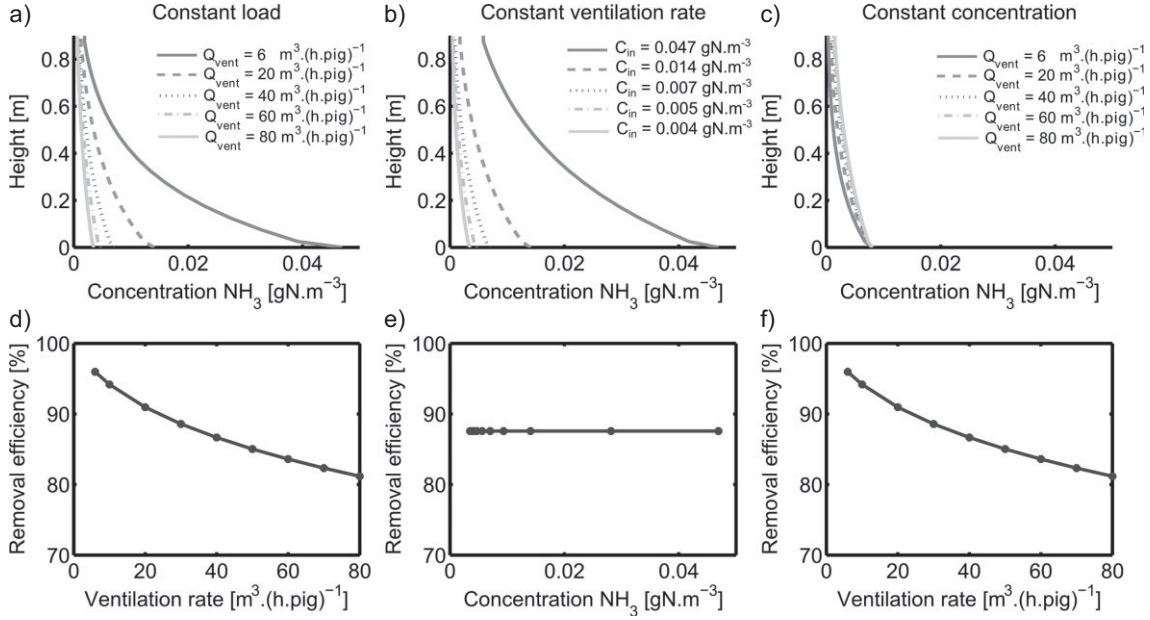

Figure 5. Simulated influence of the ventilation rate at constant load (a, d), different incoming concentrations at constant ventilation rate (b, e), and different ventilation rates at constant incoming concentration (c, f) on the ammonia gas profile in the air scrubber and the ammonia removal efficiency, respectively.

ble (higher H) but the mass transfer will increase (higher K_L), effects that counteract each other. An air temperature increase from 20 to 25 °C results in a 20.02 % higher H and a 20.11 % higher K_L, illustrating the negligible overall effect. Additionally, the acidity constant of ammonia increases at increasing temperature, implying a decreased driving force. A negligible effect of the temperature on the ammonia removal efficiency was also reported in tests of an acid spray scrubber [48] and an ammonia regeneration scrubber [49]. Additionally, by considering the heat and water balance in this study, it was possible to simulate the increased rate of water loss in the air scrubber, preceded by a higher condensation (negative evaporation) after startup of the air scrubber (Fig. 6).

5.3.3 Relative Humidity

While the effect of the relative humidity on the removal efficiency of pollutants was very small (less than 1 % difference between 45 and 99 %, results not shown), its effect on water loss

through evaporation was found significant. A high relative humidity implied a high water vapor pressure in the incoming air and thus a lower driving force for evaporation. Given that there was less evaporation, also the latent heat transfer decreased, resulting in a smaller temperature difference between the incoming and outgoing air. The equilibrium temperature of both the gas and the liquid phases inside the air scrubber was therefore higher. The water loss was much lower at higher relative humidity (Fig. 7). A comparable linearly decreasing water loss with increasing relative humidity was found by Shah et al. [49]. After startup, a higher increase in condensation occurred at higher relative humidity because the incoming water vapor pressure was already higher than the saturated vapor pressure, meaning that the temperature first needed to increase before water was evaporated (Fig. 7).

5.4 Influence of the Design

Using a packing material with a higher specific surface area resulted in increasing removal efficiency (Fig. 8) as more contact surface area was available for mass and heat transfer and the mass transfer coefficient increased (Fig. 2). In practice, however, the specific surface area cannot be increased too much to avoid the risk of clogging due to the formation of ammonium salts. Accumulated ammonium salts will also decrease the specific surface area during operation, implying that the removal efficiency will decrease accordingly.

Fig. 8 displays the influence of the specific surface area and packing dimensions on the ammonia removal efficiency. Increasing the volume of the packing material resulted in increased removal efficiency. With respect to the effect of the cross-section, only its area influences the removal efficiency while the aspect ratio does not. Increasing the cross-sectional area of the packing resulted in a smaller positive effect than increasing its height, for the same contact area above 594 m^2 (reference case). This is explained by the decreased gas velocity associated with an increased cross-sectional area, reducing the mass transfer coefficient (Eq. (12)). It can further be noted that changing the dimensions of the air scrubber will also affect the pressure drop, which strongly influences the energy cost. Increasing the height of the air scrubber (for a constant packing volume) increases the ammonia removal efficiency, but reduces the cross-sectional area and thus increases the pressure drop; doubling the air velocity through the scrubber quadruples the pressure drop [50]. The optimal packing height will compromise the maximal removal efficiency and the minimal pressure drop.

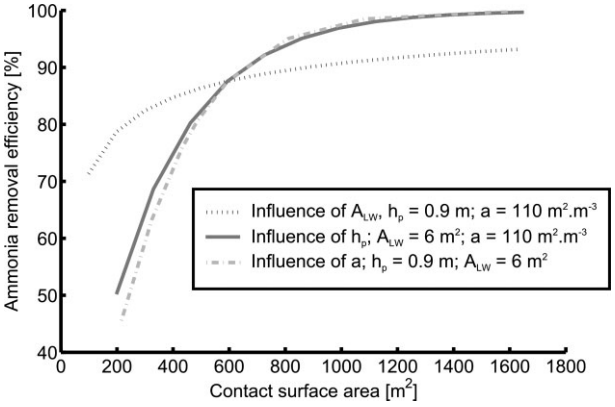

Figure 8. Simulated influence of the air scrubber packing dimensions (height h in m and cross-sectional area A in m^2) and the specific surface area (a in m^2m^{-3}) on the ammonia removal efficiency.

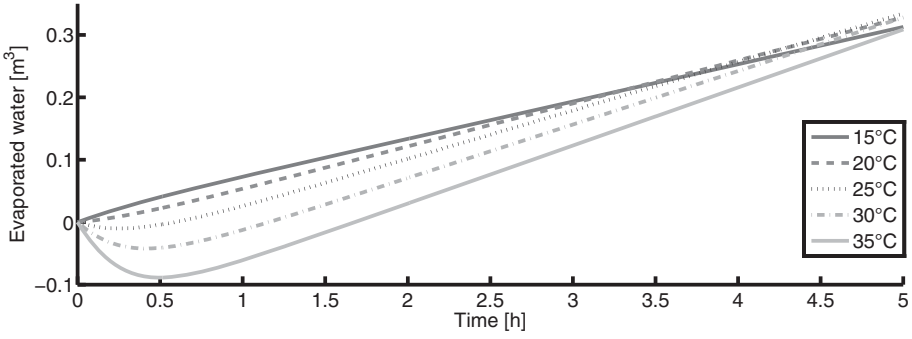

Figure 6. Simulated influence of the air temperature on the water loss in the air scrubber.

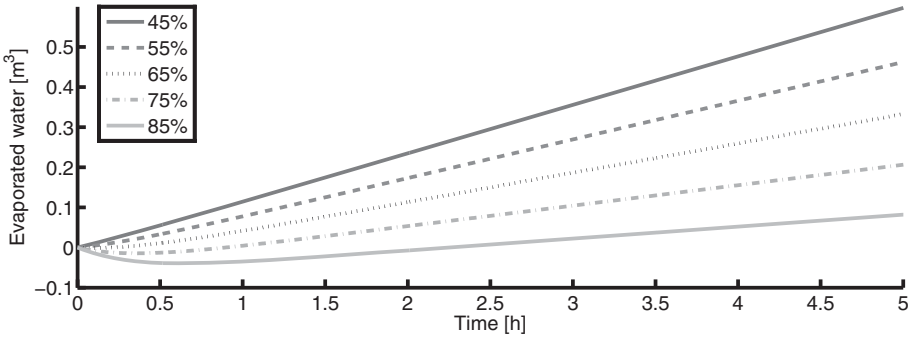

Figure 7. Simulated influence of the relative humidity on the water loss in the air scrubber.

5.5 Influence of Operational Variables

A small increase in the pH near the pK_a ($pK_a = 9.24$ [51]) at which a shift occurs from ammonium to ammonia will cause a significant decrease in the ammonia removal efficiency (Fig. 9). The removal efficiency of H_2S, being an acid ($pK_a = 7.02$ [51]), is influenced by the pH in the opposite way as for NH_3 (results not shown). Nevertheless, the maximum removal efficiency that could be reached, at pH = 14, was still only 1.4 % compared to 0 % in the reference case. This is related to the high Henry

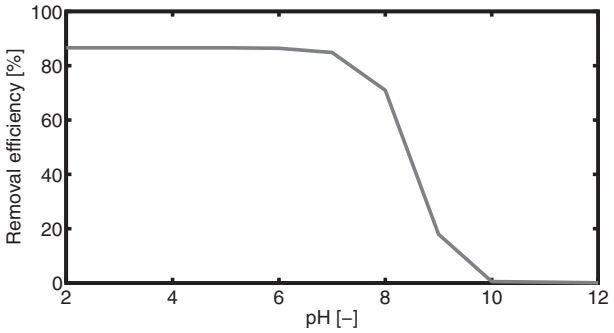

Figure 9. Simulated influence of the pH on the ammonia removal efficiency.

coefficient of H_2S (low solubility) and the low residence time applicable in air scrubbers for agricultural use.

At increasing liquid flow rate, the mass transfer coefficient increased, leading to increased removal efficiency (results not shown). However, the latter increase was very small (only 1.2 % between 0.4 and 35 $m^3m^{-2}h^{-1}$. Since only a very small improvement in removal efficiency is observed with increasing liquid flow rates, the flow rate can be kept as low as possible to reduce the pumping cost for recirculation while keeping the packing material completely wet.

6 Conclusions

A mechanistic model for a countercurrent chemical air scrubber was set up based on the concentrations of incoming pollutants, the air temperature, and the relative humidity. Model evaluation through simulation showed the following:

- The model is able to predict the removal efficiency, the gas and liquid temperature profiles, the relative humidity profile, and the evaporation rate at the same time. It thus provides a useful tool for further process optimization in terms of design and control.
- The choice of the correlations for both the gas and liquid mass transfer coefficients significantly affects the simulation results; their selection requires specific attention.
- The model was validated for typical conditions prevailing in pig housing facilities in Flanders. The model was able to describe the experimental results with an average difference for the outgoing ammonia concentration, the air temperature, and the relative humidity of 14, 5, and 5 %, respectively.
- The ammonia removal efficiency increases with decreasing pH of the washing liquid as well as with increasing packing volume or specific surface area. A higher increase is achieved by increasing the packing height rather than its length or width, for the same contact surface area.
- The water consumption increases with increasing temperature and decreasing relative humidity of the incoming gas stream, while they hardly affect the removal efficiency.
- The ventilation rate has a significant influence on both the removal efficiency and the water consumption. Higher ventilation rates lead to decreasing removal efficiency because of a decreased contact time rather than because of dilution of the incoming air.

Acknowledgment

C. Van der Heyden was financially supported by the Special Research Fund (BOF) of Ghent University (project number 01N02012), the Institute for Agriculture and Fisheries Research (ILVO), and through a Ph.D. fellowship of the Agency for Innovation by Science and Technology (IWT; project number SB-131586).

The authors have declared no conflict of interest.

Symbols used

a	[m^2m^{-3}]	specific surface area
A_{LW}	[m^2]	cross-sectional area, $w_p l_p$
cp_G	[–]	packing specific coefficient for the gas phase
cp_L	[–]	packing specific coefficient for the liquid phase
c_p	[$J\,kg^{-1}K^{-1}$]	specific heat
C	[$g\,m^{-3}$]	concentration
d_h	[m]	hydraulic diameter of the packing
d_p	[m]	particle diameter
D	[m^2s^{-1}]	diffusion constant
EC	[$S\,m^{-1}$]	electrical conductivity
EF	[$kg\,animal^{-1}a^{-1}$]	load
f	[–]	fraction
g	[$m\,s^{-2}$]	acceleration of gravity
h	[$W\,m^{-2}K^{-1}$]	heat transfer coefficient
h_L	[m^3m^{-3}]	liquid holdup of the packing
h_p	[m]	height of the packing
H	[–]	Henry coefficient (gas to water)
ΔH_V	[$J\,kg^{-1}$]	evaporation enthalpy
k	[$m\,s^{-1}$]	mass transfer coefficient
K_L	[$m\,s^{-1}$]	overall mass transfer coefficient
K_a	[$mol\,m^{-3}$]	acidity constant
l_p	[m]	length of the packing
M	[$g\,mol^{-1}$]	molecular weight
n_{pigs}	[animal]	number of pigs
Nu	[–]	Nusselt number
nY	[–]	number of cells
p	[Pa]	pressure
Pe	[–]	Peclet number
Pr	[–]	Prandtl number
Q	[m^3s^{-1}]	flow rate
R	[$J\,K^{-1}mol^{-1}$]	gas constant
RH	[%]	relative humidity
Sc	[–]	Schmidt number
Sh	[–]	Sherwood number
t	[s]	time
T	[°C]	temperature
u	[$m\,s^{-1}$]	velocity
V	[m^3]	volume
w_p	[m]	width of the packing
y	[m]	film thickness

Greek letters

ε	[–]	void fraction of the packing
λ	[W m^{-1}K^{-1}]	thermal conductivity
μ	[Pa s]	dynamic viscosity
ρ	[kg m^{-3}]	volumetric concentration, volumetric mass

Sub-/superscripts

BT	buffer tank
D	discharge
EW	evaporated water
F	fluid (gas or liquid)
FW	fresh water
G	gas
i	cell number *i*
in	inlet
int	interface
L	liquid
out	outlet
p	packing of the air scrubber
R	recirculation
st	steam
sv	saturated water vapor
v	water vapor
vent	ventilation

References

[1] K. B. Schnelle Jr., C. A. Brown, *Air Pollution Control Technology Handbook*, CRC Press, Boca Raton, FL **2002**.

[2] R. K. Srivastava, W. Jozewicz, *J. Air Waste Manage. Assoc.* **2001**, *51*, 1676–1688.

[3] C. Van der Heyden, P. Demeyer, E. I. P. Volcke, *Biosyst. Eng.* **2015**, *134*, 74–93.

[4] B. D. Thomas, S. Colle, J. Vanderschuren, *Chem. Eng. Technol.* **2003**, *26*, 497–502.

[5] T. W. Chien, H. Chu, H. T. Hsueh, *J. Environ. Eng.* **2003**, *129*, 967–974.

[6] S. Roy, G. T. Rochelle, *Sep. Sci. Technol.* **2004**, *39*, 3057–3077.

[7] L. S. Hadlocon, L. Y. Zhao, R. B. Manuzon, I. E. Elbatawi, *Trans. ASABE* **2014**, *57*, 949–960.

[8] J. Hahne, K. D. Vorlop, *Landbauforsch. Völkenrode* **2001**, *51*, 121–130.

[9] *Best Available Techniques (BAT) Reference Document for the Intensive Rearing of Poultry or Pigs*, final draft, European Commision, Seville **2015**. http://eippcb.jrc.ec.europa.eu/reference/BREF/IRPP_Final_Draft_082015_bw.pdf

[10] R. W. Melse, N. W. M. Ogink, *Trans. ASAE* **2005**, *48*, 2303–2313.

[11] E. Y. Kenig, L. Kucka, A. Górak, *Chem. Eng. Technol.* **2003**, *26*, 631–646.

[12] S. Kiil, M. L. Michelsen, K. Dam-Johansen, *Ind. Eng. Chem. Res.* **1998**, *37*, 2792–2806.

[13] O. Brettschneider, R. Thiele, R. Faber, H. Thielert, G. Wozny, *Sep. Purif. Technol.* **2004**, *39*, 139–159.

[14] F. Bashipour, S. N. Khorasani, A. Rahimi, *Chem. Eng. Technol.* **2015**, *38*, 2137–2145.

[15] M. Meyer, M. Hendou, M. Prevost, *Comput. Chem. Eng.* **1995**, *19*, S277–S282.

[16] T. J. Overcamp, *Environ. Sci. Technol.* **1999**, *33*, 155–156.

[17] H. Perez-Blanco, in *Winter Meeting of the American Society of Heating, Refrigerating and Air-Conditioning Engineers*, Dallas, TX **1988**, 467–483.

[18] H. Yoon, J. Lim, H. Chung, *Bull. Korean Chem. Soc.* **2008**, *29*, 555–561.

[19] A. Shanableh, M. Imteaz, *Bull. Korean Chem. Soc.* **2010**, *31*, 1920–1926.

[20] C.-H. Huang, *Environ. Eng. Sci.* **2005**, *22*, 535–541.

[21] K. Ocfemia, Y. Zhang, Z. Tan, *Trans. ASAE* **2005**, *48*, 1561–1566.

[22] P. Khakharia et al., *Ind. Eng. Chem. Res.* **2014**, *53*, 13195–13204.

[23] G. F. Froment, K. B. Bischoff, *Chemical Reactor Analysis and Design*, 2nd ed., John Wiley & Sons, Hoboken, NJ **1990**.

[24] E. A. Foumeny, H. Pahlevanzadeh, *Chem. Eng. Technol.* **1990**, *13*, 161–171.

[25] S. V. Patankar, *Numerical Heat Transfer and Fluid Flow*, Series in Computational Methods in Mechanics and Thermal Sciences, Hemisphere Publishing, New York **1980**.

[26] S. Kim, M. Deshusses, *Environ. Prog.* **2003**, *22*, 119–128.

[27] F. Montes, C. A. Rotz, H. Chaoui, *Trans. ASABE* **2009**, *52*, 1707–1719.

[28] P. K. Dasgupta, S. Dong, *Atmos. Environ.* **1985**, *20*, 565–570.

[29] D. Liu, A. Feilberg, A. M. Nielsen, A. P. S. Adamsen, *Chemosphere* **2013**, *90*, 1396–1403.

[30] W. K. Lewis, W. G. Whitman, *Ind. Eng. Chem. Res.* **1924**, *16*, 1215–1220.

[31] T. Ibusuki, V. P. Aneja, *Chem. Eng. Sci.* **1984**, *39*, 1143–1155.

[32] G. Q. Wang, X. G. Yuan, K. T. Yu, *Ind. Eng. Chem. Res.* **2005**, *44*, 8715–8729.

[33] R. R. Andreasen, D. Liu, S. Ravn, A. Feilberg, T. G. Poulsen, *Chem. Eng. J.* **2013**, *220*, 431–440.

[34] P. V. Roberts, G. D. Hopkins, C. Munz, A. H. Riojas, *Environ. Sci. Technol.* **1985**, *19*, 164–173.

[35] E. L. Cussler, *Diffusion: Mass Transfer in Fluid Systems*, 3rd ed., Cambridge Series in Chemical Engineering, Cambridge University Press, Cambridge **2009**.

[36] K. Onda, H. Takeuchi, Y. Okumoto, *J. Chem. Eng. Jpn.* **1968**, *1*, 56–62.

[37] H. L. Shulman, C. F. Ullrich, A. Z. Prouxl, J. O. Zimmerman, *AIChE J.* **1955**, *1*, 253–258.

[38] R. Billet, M. Schultes, *Chem. Eng. Res. Des.* **1999**, *77*, 498–504.

[39] T. H. Chilton, A. P. Colburn, *Ind. Eng. Chem. Res.* **1934**, *26*, 1183–1187.

[40] R. W. Melse, N. W. M. Ogink, W. H. Rulkens, *Biosyst. Eng.* **2009**, *104*, 289–298.

[41] M. J. Hansen, A. P. S. Adamsen, P. Pedersen, A. Feilberg, *J. Environ. Qual.* **2012**, *41*, 436–443.

[42] Kenniscentrum InfoMil, *Overview of All Housing Systems (Leaflets) and the Emission Factor per Animal Category*, Rijkswaterstaat Environment, Rijswijk, **2015**. www.infomil.nl/onderwerpen/landbouw-tuinbouw/ammoniak/rav/stalbeschrijvingen/ (accessed on June 30, 2015)

[43] H. H. Ellen, J. M. G. Hol, A. I. J. Hoofs, J. Mosquera, *Comparison Theory and Practice of Emission Reduction by Chem-*

ical Air Scrubbers with Bypass Fans (in Dutch), Report 74, Animal Science Group van Wageningen UR, Wageningen **2007**.

[44] R. W. Melse, H. C. Willers, *Application of Air Cleaning Techniques in the Intensive Livestock Sector. Phase 1: Technique and Costs* (in Dutch), Report 029, Agrotechnology & Food Innovations, Wageningen **2004**.

[45] R. W. Melse, N. W. M. Ogink, *Application of Air Cleaning Techniques in the Intensive Livestock Sector. Phase 2: Possibilities for Costs Reduction of Scrubbers* (in Dutch), Report 271, Agrotechnology & Food Innovations, Wageningen **2004**.

[46] *Een luchtwasser, wat nu?*, Innovatiesteunpunt, Inagro, VCM, Provincie Vlaams-Brabant, **2014**. www.vlaamsbrabant.be/binaries/publicatie-luchtwasser-2014-brochure_tcm5-97725.pdf

[47] T. Ulens, S. Millet, N. Van Ransbeeck, S. Van Weyenberg, H. Van Langenhove, P. Demeyer, *Livest. Sci.* **2014**, *159*, 123–132.

[48] R. B. Manuzon, L. Y. Zhao, H. M. Keener, M. J. Darr, *Trans. ASABE* **2007**, *50*, 1395–1407.

[49] S. B. Shah, P. W. Westerman, R. D. Munilla, M. E. Adcock, G. R. Baughman, *Trans. ASABE* **2008**, *51*, 243–250.

[50] R. R. Andreasen, T. G. Poulsen, *J. Environ. Eng.* **2013**, *139*, 196–204.

[51] D. A. Skoog, D. M. West, F. J. Holler, S. R. Crouch, *Analytical Chemistry: An Introduction*, 7th ed., Brooks/Cole, Cengage Learning, Belmont, CA **2000**.

